

OPEN ACCESS

Communication—Proving the Importance of Pt-Interlayer Position in PEMWE Membranes for the Effective Reduction of the Anodic Hydrogen Content

To cite this article: Agate Martin *et al* 2021 *J. Electrochem. Soc.* **168** 094509

View the [article online](#) for updates and enhancements.



*Benefit from connecting
with your community*

ECS Membership = Connection

ECS membership connects you to the electrochemical community:

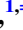







- Facilitate your research and discovery through ECS meetings which convene scientists from around the world;
- Access professional support through your lifetime career;
- Open up mentorship opportunities across the stages of your career;
- Build relationships that nurture partnership, teamwork—and success!

Join ECS! **Visit electrochem.org/join**





Communication—Proving the Importance of Pt-Interlayer Position in PEMWE Membranes for the Effective Reduction of the Anodic Hydrogen Content

Agate Martin,^{1,=}  Dunia Abbas,^{2,3,=}  Patrick Trinke,¹  Thomas Böhm,² 
Markus Bierling,^{2,3}  Boris Bensmann,^{1,z}  Simon Thiele,^{2,3}  and Richard Hanke-Rauschenbach¹ 

¹Leibniz University Hannover, Institute of Electric Power Systems, 30167 Hannover, Germany

²Forschungszentrum Jülich GmbH, Helmholtz Institute Erlangen-Nürnberg for Renewable Energy (IEK-11), 91058 Erlangen, Germany

³Department of Chemical and Biological Engineering, Friedrich-Alexander-Universität Erlangen-Nürnberg, 91058 Erlangen, Germany

Gas crossover through the membrane poses a significant challenge to proton exchange membrane water electrolyzers. This work investigates the influence of the position of platinum-based recombination interlayers integrated in the membrane on the anodic hydrogen in oxygen content. The results show that all interlayer positions reduce the anodic hydrogen content without performance losses compared to the reference without interlayer. However, an interlayer positioned closer to the anode is more effective than closer to the cathode. Further, the effect of the interlayer is more pronounced with increasing anode pressure.

© 2021 The Author(s). Published on behalf of The Electrochemical Society by IOP Publishing Limited. This is an open access article distributed under the terms of the Creative Commons Attribution 4.0 License (CC BY, <http://creativecommons.org/licenses/by/4.0/>), which permits unrestricted reuse of the work in any medium, provided the original work is properly cited. [DOI: 10.1149/1945-7111/ac275b]



Manuscript submitted July 14, 2021; revised manuscript received September 1, 2021. Published September 24, 2021.

Proton exchange membrane water electrolysis (PEMWE) is an emerging technology for the production of green hydrogen. Major technology goals are improved system reliability especially in dynamic operation, the operation at elevated cathode pressure, and the reduction of membrane thickness.^{1–3} However, with increasing operating pressure as well as with decreasing membrane thickness, hydrogen crossover from cathode to anode through the membrane increases^{4–6} and results in the formation of explosive gas mixtures for H₂ in O₂ contents above 4 vol.%.⁷ Therefore, PEM electrolyzers are typically operated up to a safety limit around 2 vol.% H₂ in O₂.^{1,3,7,8} Research activities have focused on different strategies to limit the H₂ in O₂ content in PEM electrolyzers,⁶ e.g. by integrating recombination catalysts i) in the gas separator,⁸ ii) directly on the anode⁹ or iii) inside the membrane.¹⁰ The latter work has shown that a platinum interlayer reduced the anodic H₂ in O₂ content significantly. It also provided a theoretical assessment of the ideal position of a recombination layer for the reduction of both, hydrogen and oxygen gas fluxes across the membrane.

The present work studies the influence of the Pt-interlayer position on the H₂ in O₂ content experimentally. Catalyst coated membranes (CCMs) with recombination interlayers (IL) close to the anode (IL_{an}), in the middle (IL_{mid}), close to the cathode (IL_{cat}) and a reference without interlayer (no_IL) were fabricated and examined regarding their polarisation behaviour and hydrogen crossover properties at different pressure conditions.

Materials and Methods

Catalyst Coated Membranes.—Spray-Coating of Membranes.—A spray coater (Sono-Tek) was used to fabricate Nafion membranes onto a PTFE substrate. A dispersion of Nafion D2021 (FuelCellStore) and isopropanol in a weight ratio of 3.34/10 was mixed. For the Pt-interlayers, a mixture of Pt-nanoparticles (Sigma-Aldrich, particle size < 50 nm), Nafion D2020 (FuelCellStore) and isopropanol in a weight ratio of 0.0043/1.43/10 was stirred for 48 h. Nafion layers were sprayed with a flow rate of 0.9 ml min⁻¹ and a nozzle speed of 100 mm s⁻¹ at 65 °C to ensure complete solvent evaporation. For no_IL, 36 consecutive spray runs were conducted. For IL_{an} and

IL_{cat}, 30 spray runs were performed, while 17 runs were required for IL_{mid}. Subsequently, the Pt-interlayer was deposited in 22 runs with a flow rate of 0.3 ml min⁻¹ and a nozzle speed of 140 mm s⁻¹. A second Nafion layer was then deposited on top of the membranes (IL_{an} and IL_{cat} in 4 runs; IL_{mid} in 17 runs). The Pt-loading was determined based on the weight gain as 0.01 mg_{Pt} cm⁻². The final membrane thickness in the dry state yielded 110 ± 5 μm.

Electrode Fabrication.—Decal electrodes with loadings of 0.16 ± 0.05 mg_{Pt} cm⁻² (with I/C = 0.65) for the cathode and 2 ± 0.3 mg_{Ir} cm⁻² (with I/C = 0.13) for the anode were fabricated using Nafion D2021 (FuelCellStore) as binder, TEC10V40E (Tanaka) as cathode catalyst and Elyst Ir75 (Umicore) as anode catalyst. CCMs were fabricated by hot pressing 4 cm² electrodes onto the membranes at 160 °C at a pressure of 2 MPa for 5 min.

Test Setup.—Cell Assembly.—The used 4 cm² cell, designed by Fraunhofer ISE,¹¹ is comprised of gold-coated titanium blocks and is equipped with PEEK isolation frames and flat sealings (60FC-FKM200, 0.8 mm, Freudenberg). The contact force was monitored with a load cell (K-14, GM77, Lorenz Messtechnik GmbH).

On the cathode, a carbon porous transport layer (PTL, H2312, 210 μm, Freudenberg) and on the anode a titanium PTL (1 mm, grade 1, 2GDL40–1.00, Bekaert) were used. The CCMs were assembled in dry state in the cell.

Testing Periphery.—The measurements were performed with an E100 test station (Greenlight Innovation). A BCS815 potentiostat (BioLogic) was used as current source. The analysis of the dried anodic product gas with a gas chromatograph (GC, 490 μGC System, Agilent) is described in Refs. 6, 10 and 12.

As high hydrogen contents were expected at low current densities and high cathode pressures, the anode product gas was diluted with an additional flow of oxygen (0.04 g min⁻¹ or N_{O₂}^{dil} = 2.167 · 10⁻⁵ mol s⁻¹) applied with a mass flow controller (EL-FLOW Prestige, Bronkhorst) directly behind the anode outlet.

Measurement Protocol.—After cell assembly, the cell was mounted into the test station and was conditioned thermally for 1 h at the measurement temperature of 80 °C. Then, the compression force of 4 kN was applied.

⁼These authors contributed equally to this work.

^zE-mail: boris.bensmann@ifes.uni-hannover.de

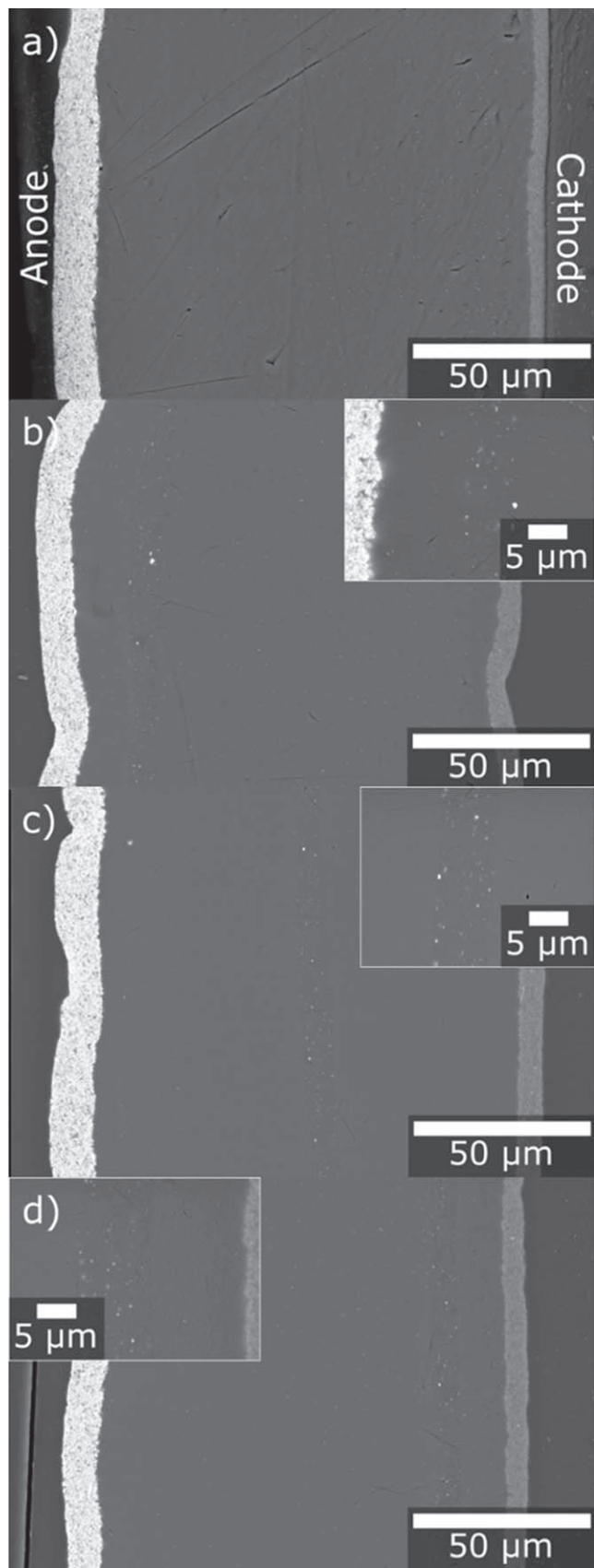


Figure 1. Cross-sections of (a) no_IL, (b) IL_an, (c) IL_mid, and (d) IL_cat after electrochemical characterisation. Additional insets with higher magnification for a representation of the Pt-interlayers are provided.

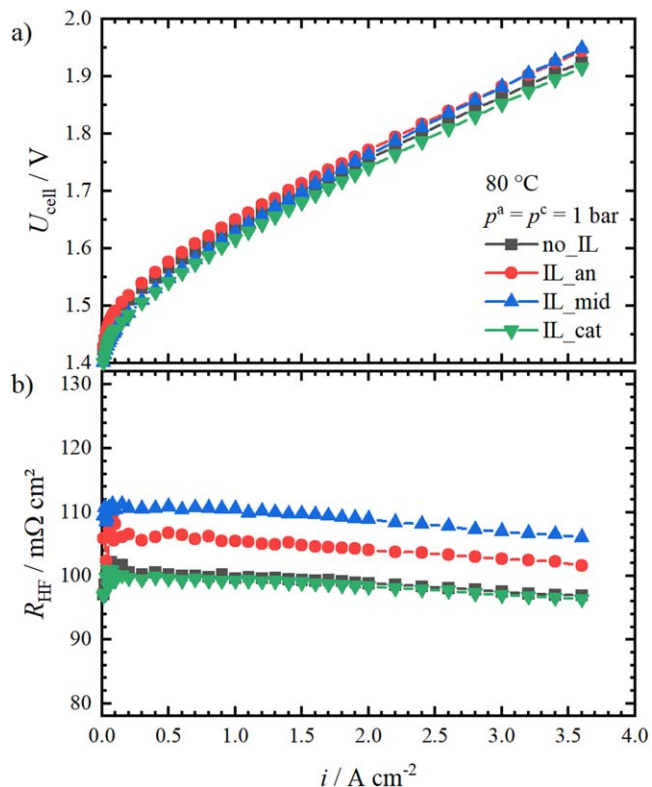


Figure 2. Polarisation behaviour of all investigated CCMs in (a) and their R_{HF} in (b).

Hydrogen Crossover.—A galvanostatic step profile of eight current density steps from 0.1 A cm^{-2} to 3.5 A cm^{-2} was used for monitoring the H_2 in O_2 content via GC. Each current density was held until a constant GC-signal was reached.

This procedure was repeated for three absolute pressure combinations ($p^c = 1 \text{ bar}$ and $p^a = 1 \text{ bar}$, $p^c = 10 \text{ bar}$ and $p^a = 1 \text{ bar}$, $p^c = 10 \text{ bar}$ and $p^a = 5 \text{ bar}$). At ambient pressure, two cycles were performed in order to purge the test station.

Polarisation Behaviour.—After the crossover measurements, polarisation curves were recorded from 0.01 A cm^{-2} to 3.6 A cm^{-2} in logarithmic steps until 2 A cm^{-2} and then with steps of 0.2 A cm^{-2} . The holding time was 10 s per step. For the determination of the high frequency resistance R_{HF} , each current step was followed by an electrochemical impedance measurement between 10 kHz and 100 Hz and a current amplitude of 10%. R_{HF} was obtained by interpolating the Nyquist plots at the intercept with the real axis. The measurement was repeated three times and the third cycle was used for evaluation.

SEM Cross-Sections.—Cross-sections of *post mortem* CCMs were prepared by embedding the samples in epoxy resin, followed by grinding and polishing of the embedded samples. The cross-sections were imaged by SEM (Zeiss Crossbeam 540, BSD detector) after Au-sputtering.

Results and Discussion

SEM Cross-Sections.—Figure 1 shows cross-sections of the tested CCMs after disassembly of the cells. The overall membrane thicknesses range from 110 to $120 \mu\text{m}$. The Pt-interlayers show thicknesses of approximately 7 to $12 \mu\text{m}$ close to the anode (Fig. 1b), in the middle (Fig. 1c), and close to the cathode (Fig. 1d).

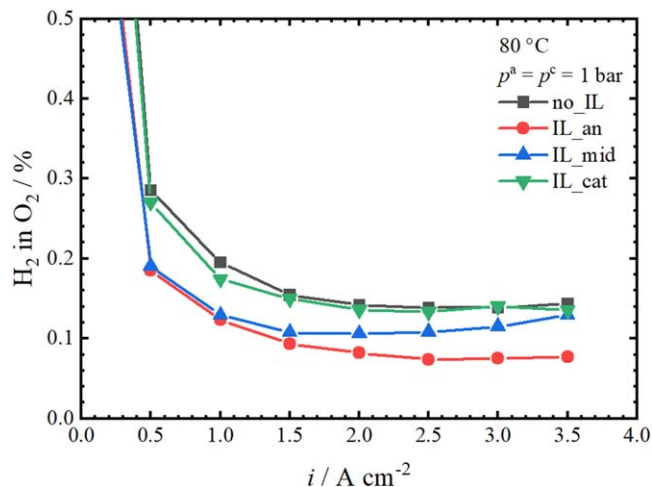


Figure 3. H₂ in O₂ contents of the investigated CCMs at ambient pressure.

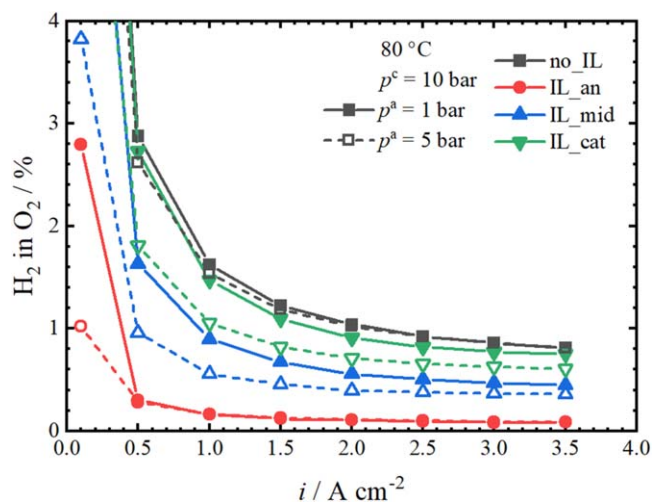


Figure 4. H₂ in O₂ contents at elevated cathode pressure $p^c = 10$ bar and different anode pressures: $p^a = 1$ bar (filled symbols) and $p^a = 5$ bar (hollow symbols).

Polarisation Behaviour.—The measured cell polarisation behaviour at 80 °C and ambient pressure is shown in Fig. 2. All CCMs show similar and good electrochemical performance with voltages below 2 V even at high current densities (Fig. 2a). The maximum voltage deviation at 3.6 A cm⁻² is 33 mV.

The ohmic resistance of the interlayer membranes are approximated with the measured high frequency resistance R_{HF} . As displayed in Fig. 2b), R_{HF} decreases slightly with current density. This temperature effect was already explained previously.^{13,14} IL_{mid} shows the highest R_{HF} (110 mΩ cm² at 1 A cm⁻²), whereas IL_{cat} shows the lowest value (99 mΩ cm² at 1 A cm⁻²). The differences between the R_{HF} values might be attributed to slight deviations in membrane thicknesses or tolerances due to cell assembly. Nonetheless, all measured R_{HF} values comply with literature values for slightly thicker commercial Nafion membranes (~110 mΩ cm² for N115).^{12,15} Hence, the incorporation of the Pt-interlayer into the membrane has no apparent effect on R_{HF} . This is in contrast to the previous work of Klose *et al.*¹⁰ and may result from the reduced loading or an improved manufacturing process.

In summary, these results show that the integration and the position of a Pt-interlayer into the membrane does not significantly affect the electrochemical polarisation behaviour. The minor deviations provide a good base for evaluation of the CCMs with regards to their crossover properties.

Hydrogen crossover.—The Pt-interlayers in the membranes are intended to function as a recombination layer for permeating product gases. For the evaluation of their recombination abilities, the anodic hydrogen content is used as a measure. Since the anodic product gas was diluted with an additional oxygen flux $N_{O_2}^{dil}$, the measured hydrogen content at the GC $\phi_{H_2}^{GC}$ is described by Eq. 1, where the evolved oxygen flux equals $N_{O_2}^{evo} = \frac{i}{4 \cdot F}$ and $N_{H_2}^{cross}$ is the hydrogen crossover flux.

$$\phi_{H_2}^{GC} = \frac{N_{H_2}^{cross}}{N_{O_2}^{evo} + N_{O_2}^{dil} + N_{H_2}^{cross}} \quad [1]$$

The real hydrogen content $\phi_{H_2}^{real}$ can be determined by converting Eq. 1 to $N_{H_2}^{cross}$ and inserting it then into Eq. 2.

$$\phi_{H_2}^{real} = \frac{N_{H_2}^{cross}}{N_{O_2}^{evo} + N_{H_2}^{cross}} = \frac{\phi_{H_2}^{GC} \cdot (N_{O_2}^{evo} + N_{O_2}^{dil})}{N_{O_2}^{evo} + \phi_{H_2}^{GC} \cdot N_{O_2}^{dil}} \quad [2]$$

Figure 3 shows the resulting H₂ in O₂ content for ambient pressure operation. The hydrogen content follows the expected qualitative course for all four experiments. As expected, the highest hydrogen contents are obtained with no_IL. Using IL_{cat} leads to contents in a similar range. With the other two samples (IL_{an} and IL_{mid}), noticeably lower hydrogen contents are obtained. The lowest values are obtained with IL_{an}. At 3 A cm⁻², a reduction of 43% (from 0.14% to 0.08%) was achieved with this CCM. Since hydrogen is still detected on the anode, the loading of the recombination catalysts, and thus the available catalyst surface area, might be too small or the oxygen crossover is not high enough for a complete recombination of hydrogen at the Pt-interlayer.

The impact of the interlayer positioning on the anodic hydrogen content is more pronounced at an elevated cathode pressure of 10 bar combined with atmospheric anode pressure, as seen in Fig. 4. Here, the content remains the highest when no interlayer is used.

The differences in hydrogen content between the CCMs with and without interlayer result from the fact that the amount of available oxygen and hydrogen at the interlayer depends on the interlayer position. Generally, the total amount of oxygen available by permeation through the membrane is less than that of hydrogen. First, the produced amount of oxygen is only half of that of hydrogen. Second, considering that most of the gas permeates in the aqueous phase of the membrane, less oxygen than hydrogen permeates, since the diffusivity of oxygen in water is lower than of hydrogen.^{4,16,17} Therefore, it can be assumed that more hydrogen recombines in the vicinity of the anode due to the higher oxygen concentration.

Up to this point, it can be summarized that for electrolysis operation under ambient anode conditions, an interlayer near the anode achieves the greatest impact regarding the reduction of the anodic H₂ in O₂ content. Consequently, the available oxygen amount at the recombination interlayer is identified as a crucial factor for the recombination reaction.

In a further experiment, it was therefore investigated how an increase of the oxygen concentration affects the recombination efficiency of the different interlayer positions. This was achieved by elevating the anode pressure from ambient to 5 bar, whereas the cathode was kept at 10 bar. The resulting hydrogen contents at the anode are shown in Fig. 4.

The general trend remains: the closer the interlayer is positioned to the anode, the lower is the resulting H₂ in O₂ content. Regarding the reference case without interlayer, the elevation of anode pressure has only a minor effect, leading to nearly identical hydrogen contents.

The incorporation of any interlayer leads to a noticeable reduction of the hydrogen content, especially at low current densities up to 0.5 A cm⁻². Regarding IL_{cat}, the enhancement of oxygen

pressure reduces the hydrogen content by 34% at 0.5 A cm⁻² compared to the atmospheric anode operation (from 2.73% to 1.81%). For IL_mid, the enhanced anode pressure even leads to a reduction of 41% (from 1.63% to 0.96%). It can be assumed that a further increase in anode pressure will lead to a further reduction of the anodic hydrogen content if the interlayer is positioned in the center or closer towards the cathode.

For IL_an, a further reduction of the H₂ in O₂ content cannot be observed for higher current densities. Therefore, it can be assumed that the oxygen concentration at ambient anode pressure is already sufficiently high for the recombination at high current densities for this interlayer position. Consequently, at an anode pressure of 5 bar, there should be sufficient oxygen for a full hydrogen recombination. This finding emphasizes that the employed Pt-loading in this work is not high enough for a complete recombination of the permeating hydrogen flux in comparison to the previous work of Klose *et al.*¹⁰ who used twice the Pt-loading.

Summary

This contribution provides experimental proof for the importance and the effect of the position of recombination catalyst layers within PEMWE membranes for the reduction of the anodic hydrogen content. It was shown that the polarisation behaviour is not significantly affected by the Pt-interlayers and their positions. Furthermore, each CCM with interlayer reduced the measurable anodic hydrogen content in comparison to the reference CCM without interlayer. As expected from the theoretical assessment of Klose *et al.*¹⁰ the strongest reduction was observed with the interlayer close to the anode. This can be explained by the available amount of dissolved oxygen in the membrane, which decreases towards the cathode and leads to a higher recombination rate of hydrogen and oxygen closer to the anode. The aforementioned theoretical assessment and the experimental results in this work suggest that a recombination interlayer close to the anode is recommended, if the hydrogen crossover should be minimized for maintaining a safe anodic gas composition.

As the available amount of oxygen at the interlayer seems to be the limiting factor for the recombination reaction, two optimisation strategies are possible for a PEM electrolyser with recombination catalysts within the membrane: i) positioning the interlayer close to the anode, or ii) elevating the anode pressure, to maximize the available concentration of oxygen at the interlayer. In order to improve the recombination effect at minimal costs, the position of the interlayer, the catalyst loading and the operating conditions need to be optimized.





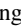
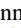

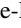
In summary, the results of this study confirm that Pt-interlayers are a suitable strategy to reduce the H₂ in O₂ content in PEMWE,

especially for thin membranes and elevated cathode pressures. This improvement can help to reduce safety issues and consolidate PEMWE as a key technology for hydrogen generation.

Acknowledgments

The authors acknowledge the financial support by the Federal Ministry of Education and Research of Germany in the framework of PowerMEM (BMBF/03EW0012).

ORCID

Agate Martin  <https://orcid.org/0000-0003-4673-1135>
 Dunia Abbas  <https://orcid.org/0000-0002-3938-0026>
 Patrick Trinke  <https://orcid.org/0000-0002-0935-5321>
 Thomas Böhm  <https://orcid.org/0000-0003-2036-2159>
 Markus Bierling  <https://orcid.org/0000-0002-4992-2095>
 Boris Bensmann  <https://orcid.org/0000-0001-8685-7192>
 Simon Thiele  <https://orcid.org/0000-0002-4248-2752>
 Richard Hanke-Rauschenbach  <https://orcid.org/0000-0002-1958-307X>

References

1. M. Schalenbach, M. Carmo, D. L. Fritz, J. Mergel, and D. Stolten, *Int. J. Hydrog. Energy*, **38**, 14921 (2013).
2. K. Ayers, N. Danilovic, R. Ouimet, M. Carmo, B. Pivovar, and M. Bornstein, *Annu. Rev. Chem. Biomol. Eng.*, **10**, 219 (2019).
3. M. Schalenbach, *Int. J. Hydrog. Energy*, **41**, 729 (2016).
4. M. Schalenbach, T. Hoefner, P. Paciok, M. Carmo, W. Lueke, and D. Stolten, *J. Phys. Chem. C*, **119**, 25145 (2015).
5. M. Bernt, J. Schröter, M. Möckl, and H. A. Gasteiger, *J. Electrochem. Soc.*, **167**, 124502 (2020).
6. P. Trinke, P. Haug, J. Brauns, B. Bensmann, R. Hanke-Rauschenbach, and T. Turek, *J. Electrochem. Soc.*, **165**, F502 (2018).
7. H. Janssen, J. C. Bringmann, B. Emonts, and V. Schroeder, *Int. J. Hydrog. Energy*, **29**, 759 (2004).
8. S. A. Grigoriev, P. Millet, S. V. Korobtsev, V. I. Porembskiy, M. Pepic, C. Etievant, C. Puyenhet, and V. N. Fateev, *Int. J. Hydrog. Energy*, **34**, 5986 (2009).
9. N. Briguglio, S. Siracusano, G. Bonura, D. Sebastián, and A. S. Aricò, *Appl. Catal. B*, **246**, 254 (2019).
10. C. Klose, P. Trinke, T. Böhm, B. Bensmann, S. Vierrath, R. Hanke-Rauschenbach, and S. Thiele, *J. Electrochem. Soc.*, **165**, F1271 (2018).
11. Fraunhofer Institute for Solar Energy Systems ISE, *Fraunhofer ISE—Annual Report 2020/2021* (Freiburg, Germany) (2021).
12. P. Trinke, G. P. Keeley, M. Carmo, B. Bensmann, and R. Hanke-Rauschenbach, *J. Electrochem. Soc.*, **166**, F465 (2019).
13. T. Schuler, T. J. Schmidt, and F. N. Büchi, *J. Electrochem. Soc.*, **166**, F555 (2019).
14. M. Suermann, T. J. Schmidt, and F. N. Büchi, *Electrochim. Acta*, **211**, 989 (2016).
15. B. Pivovar and Y. S. Kim, *J. Electrochem. Soc.*, **154**, B739 (2007).
16. T. Sakai, H. Takenaka, and E. Torikai, *J. Electrochem. Soc.*, **133**, 88 (1986).
17. H. Ito, T. Maeda, A. Nakano, and H. Takenaka, *Int. J. Hydrog. Energy*, **36**, 10527 (2011).